



# No Signature of Room Temperature Ferromagnetism in Fe-Doped ITO Thin Films

Deepannita Chakraborty<sup>1</sup> · S. Kaleemulla<sup>2</sup>

Received: 15 May 2018 / Accepted: 18 May 2018 / Published online: 8 June 2018  
© Springer Science+Business Media, LLC, part of Springer Nature 2018

## Abstract

Iron (Fe)-doped indium tin oxide thin films ( $\text{In}_{0.95-x}\text{Fe}_x\text{Sn}_{0.05}\text{O}_3$  at  $x = 0.00, 0.05, 0.10,$  and  $0.15$ ) were deposited onto glass substrates using an electron beam evaporation technique. The coated thin films were characterized by X-ray diffractometer (XRD), UV-VIS-NIR spectrophotometer, photoluminescence spectrophotometer, scanning electron microscope, and vibrating sample magnetometer to study their structural, optical, morphological, and magnetic properties, respectively. The crystallite size of the films increased from 18 to 30 nm with Fe concentration ( $x$ ). The morphology showed the formation of nanorods. The bandgap of the films decreased from 3.94 to 3.81 eV. The X-ray photoelectron spectroscopy (XPS) studies confirm the presence of Fe ions in two different oxidation states ( $\text{Fe}^{2+}, \text{Fe}^{3+}$ ). The magnetic studies revealed the paramagnetic behavior of the films at room temperature and at low temperature (5 K). The effective magnetic moment ( $\mu_{\text{eff}}$ ) of Fe-doped indium tin oxide thin films was calculated using Langevin theory of paramagnetism extending to Curie's law. The effective magnetic moment ( $\mu_{\text{eff}}$ ) was increased on increasing the dopant concentration.

**Keywords** XPS · Paramagnetism · Skyrmions · Electron beam evaporation · Shallow trapping centers · Chirality

## 1 Introduction

Currently, great interest is shown on the materials which exhibit high optical transparency, electrical conductivity along with ferromagnetic properties. Such types of materials are termed as dilute magnetic semiconductors (DMS). They find increased interest due to their potential applications in the field of spintronics. These spintronic devices should be as small as possible in dimensions as the future technology should be in handy. Hence, researchers had started showing interest towards nanotechnology and nanomaterials. The field of nanotechnology is of great importance nowadays. Now, research interest is more on thin films (2D) technology. It inspires the researchers to observe the enhancement in the physical properties of the material, when it is transferred from bulk (3D) to two dimensions (2D). The most important parameter which

makes thin film advantageous over nanoparticles is its high surface to volume ratio.

Till now, many transition metal-doped oxide semiconductors such as ZnO, TiO<sub>2</sub>, CeO<sub>2</sub>, and In<sub>2</sub>O<sub>3</sub> were found as ferromagnets at room temperature. Among them, indium oxide (In<sub>2</sub>O<sub>3</sub>) has high density of charge carriers, optical transparency, and low impact on the environment. In order to enhance the optical and electrical properties, transition metals (Sn) were doped into host In<sub>2</sub>O<sub>3</sub>. This leads to the formation of one of the best transparent conductive oxides (TCOs) namely indium tin oxide (ITO). Consequently, ITO has high optical transparency, high electrical conductivity, and high reflectance at the visible region [1–9]. ITO films have been used as transparent electrodes for flat-panel displays, electrochromic windows, solar panels, bio sensors, and solar-energy heat mirrors [2–4, 10, 11]. A large number of articles on transition metal-doped ITO thin films at substrate temperature above 450 °C have been published [12–29], but very few are published on magnetic and photoluminescence properties of transition metal (Fe) and tin-codoped indium oxide thin films with nanorod shapes.

Room temperature ferromagnetism was reported for indium oxide thin films which were annealed in the presence of air or oxygen environment [30, 31]. The occurrence of oxygen vacancy and presence of surface

✉ S. Kaleemulla  
skaleemulla@gmail.com

<sup>1</sup> Thin Films Laboratory, School of Advanced Sciences, Vellore Institute of Technology, Vellore 632014, Tamil Nadu, India

<sup>2</sup> Thin Films Laboratory, Centre for Crystal Growth, Vellore Institute of Technology, Vellore 632014, Tamil Nadu, India

defects were termed as the important criteria for exhibiting ferromagnetism [32–36]. In this paper, the reasoning for observing paramagnetism amidst the presence of oxygen vacancy in iron (Fe)-doped indium tin oxide (ITO) thin films has been discussed.

## 2 Experimental Method

The required proportions of  $\text{In}_2\text{O}_3$ ,  $\text{SnO}_2$ , and  $\text{Fe}_2\text{O}_3$  powders were weighed using a microbalance (SHIMADZU AUY 220) and ground thoroughly for 16 h using an agate mortar and pestle and then sintered at  $850\text{ }^\circ\text{C}$  for 8 h under a pressure of  $10^{-2}$  mbar using a high-temperature furnace. The results of nanopowders were reported elsewhere [37]. The prepared powders were coated on glass substrates (Corning 7059) using the electron beam evaporation technique (12A4D, HIND HIGH VACUUM). The vacuum inside the chamber was maintained at  $2 \times 10^{-6}$  mbar during coating, and the substrate temperature was maintained at  $350\text{ }^\circ\text{C}$ . The time for depositing the target materials on the substrate is taken as 30 min. The thickness of the thin films was measured using a surface profilometer and it was around 250 nm.

The structural aspects were studied using a powder X-ray diffractometer (D8 Advance PXRD, BRUKER), surface morphology was studied using field emission scanning electron microscopy (FE-SEM), and elemental analysis was confirmed by X-ray photoelectron spectroscopy (XPS, K-Alpha, Thermoelectron). The optical absorbance and transmittance were recorded using a diffused reflectance spectrophotometer (JASCO V-670). The photoluminescence (PL) property was studied using a fluorescence spectrophotometer (Hitachi F7000). The magnetic properties at room temperature and at low temperature were studied using a vibrating sample magnetometer (VSM, Lakeshore 7303).

## 3 Results and Discussion

### 3.1 Structural Properties

Figure 1a shows the X-ray diffractometer (XRD) profile of  $(\text{In}_{0.95-x}\text{Fe}_x\text{Sn}_{0.05})_2\text{O}_3$  thin films at  $x = 0.00, 0.05, 0.10,$  and  $0.15$  after fitting the diffraction peaks using Fityk software. It coincided exactly with the standard JCPDS data of  $\text{In}_2\text{O}_3$  [JCPDS No. 06-0416]. The predominant peak (2 2 2) was found at  $31.2^\circ$  in ITO thin film. The predominant peak position of  $(\text{In}_{0.90}\text{Fe}_{0.05}\text{Sn}_{0.05})_2\text{O}_3$  film was at  $31.2^\circ$ . The diffraction peak position for (2 2 2) plane of  $(\text{In}_{0.85}\text{Fe}_{0.10}\text{Sn}_{0.05})_2\text{O}_3$  and  $(\text{In}_{0.80}\text{Fe}_{0.15}\text{Sn}_{0.05})_2\text{O}_3$  shifted towards a lower diffraction angle, i.e., from  $31.2^\circ$  to  $31.17^\circ$  and  $30.7^\circ$ , respectively, as shown in Fig. 1b. The shift in the

predominant peak position to the lower angle suggests the increase of the lattice parameter. The lattice parameter was calculated, and it also increased from 9.94 to 10.00 Å on the increasing of the dopant concentration. The crystallite size is calculated using Scherrer's formula [38].

$$D = \frac{k\lambda}{\beta \cos\theta} \quad (1)$$

where  $k$  is the constant and it is 0.94 as here nanorods are formed,  $\lambda$  is the wavelength, and  $\beta$  is full width at half maximum (FWHM). The crystallite size increased from 18 to 30 nm by increasing the Fe concentration. As the ionic radii of  $\text{Sn}^{4+}$  (0.59 Å) and  $\text{Fe}^{3+}$  (0.69 Å) are less than the ionic radius of  $\text{In}^{3+}$  (0.89 Å), the substitution of dopants in the host lattice will cause deviation of the lattice constant as well as some crystal imperfections [39, 40]. The dislocation density and lattice strain affect the broadening of peaks which may affect the crystallinity. The lattice strain and dislocation density were calculated using the Williamson-Smallman formula [41].

$$\text{strain } \varepsilon = \frac{\beta \cos\theta}{4} \quad (2)$$

and the dislocation density [42] is

$$\delta = \frac{1}{D^2} \quad (3)$$

The lattice strain was found to decrease from  $25.8 \times 10^{-4}$  to  $18.1 \times 10^{-4}$  on increasing the dopant concentration. The dislocation density was also found to decrease from  $65.8 \times 10^{14}$  to  $18.3 \times 10^{14} \text{ m}^{-2}$  on increasing the Fe concentration. This suggests that the crystallinity increases on increasing the dopant concentration. The decrease in strain and dislocation density as well as the shift in the predominant peak to a lower angle supports the behavior of enhancement in the lattice constant on the increase in dopant concentration. The difference between the crystallite sizes of Fe:ITO nanopowders reported in our earlier article [37] and the Fe:ITO thin film in the present study is correlated to the confinement of grain size due to the reduction in dimension of the sample from 3D to 2D state [43].

### 3.2 Surface Morphology

Figure 2a–d shows the EDAX spectra of  $(\text{In}_{0.95-x}\text{Fe}_x\text{Sn}_{0.05})_2\text{O}_3$  thin films with  $x = 0.00, 0.05, 0.10,$  and  $0.15$  along with FE-SEM. The FE-SEM images show the formation of nanorods on the substrates. From the inset, we can see that the particles are arranged randomly in all directions. This kind of morphology was not observed in earlier reports. Using Image J software, the nanorods were determined to have a length of around 70–100 nm and breadth of  $\sim 20$ –85 nm. The particle size increases on increasing the dopant concentration, and also, the

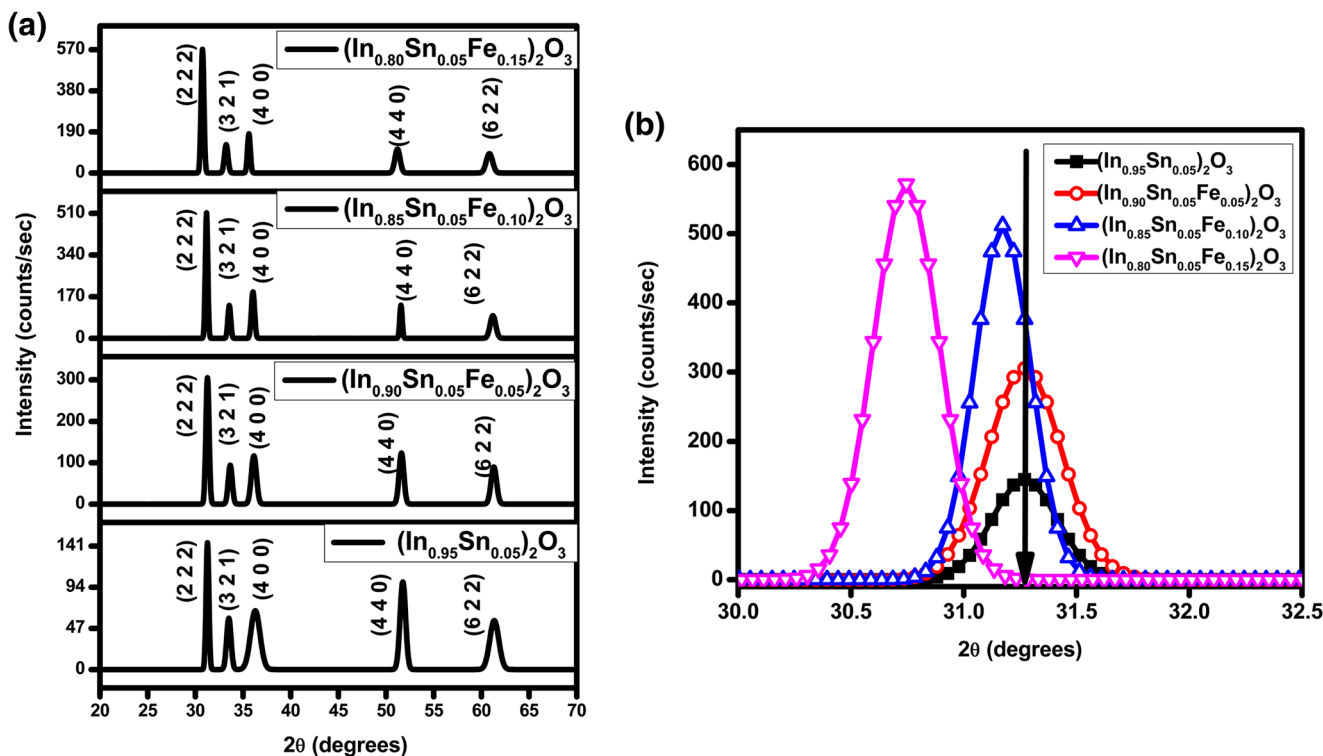


**Fig. 1** a XRD patterns of  $(\text{In}_{0.95-x}\text{Fe}_x\text{Sn}_{0.05})_2\text{O}_3$  thin films at  $x = 0, 0.05, 0.10,$  and  $0.15$ . b XRD patterns of  $(\text{In}_{0.95-x}\text{Fe}_x\text{Sn}_{0.05})_2\text{O}_3$  thin films at  $x = 0, 0.05, 0.10,$  and  $0.15$  in the  $2\theta$  range of 30 to 32°

particle size is more than the crystallite size obtained from Scherrer’s formula.

### 3.3 Optical Properties

The optical bandgaps of  $(\text{In}_{0.95-x}\text{Fe}_x\text{Sn}_{0.05})_2\text{O}_3$  thin films with  $x = 0, 0.05, 0.10,$  and  $0.15$  were determined with the

help of Tauc’s relation and shown in Fig. 3. The inset of Fig. 3 shows the optical bandgap of  $(\text{In}_{0.95}\text{Sn}_{0.05})_2\text{O}_3$  thin film. It was found that the optical bandgap decreased from 3.94 to 3.81 eV on increasing the dopant concentration of Fe. The optical bandgap energy observed here coincides with the bandgap energy obtained by Fallah et al. [43] for ITO thin films. This decrease in optical energy bandgap was

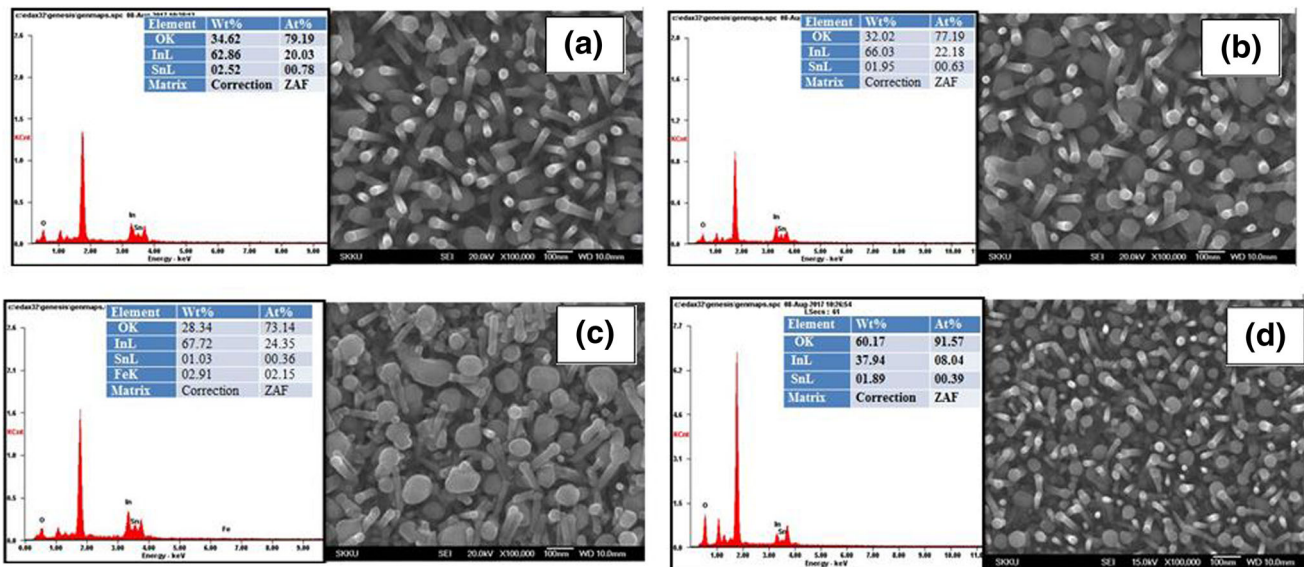
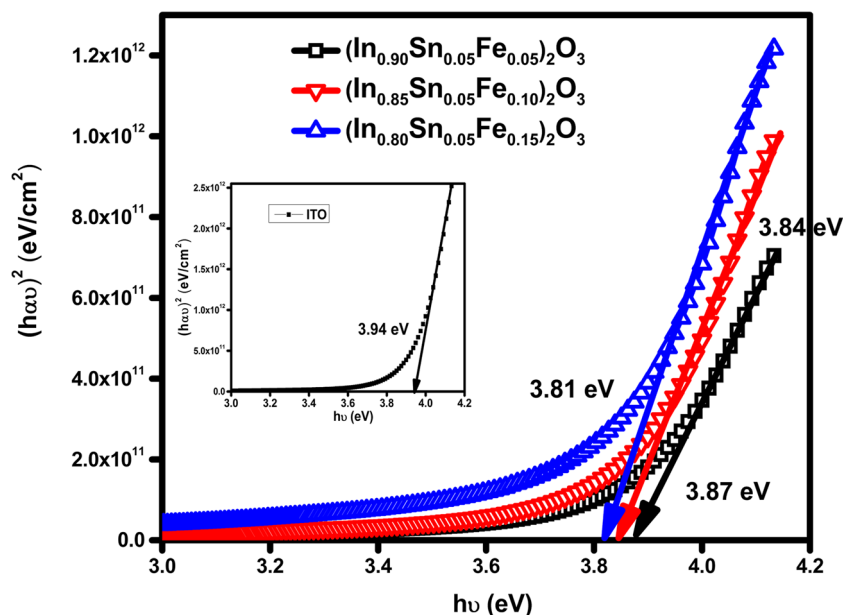


**Fig. 2** a–d EDAX spectra along with FESEM micrograph of  $(\text{In}_{0.95-x}\text{Fe}_x\text{Sn}_{0.05})_2\text{O}_3$  thin films with a  $x = 0.00$ , b  $x = 0.05$ , c  $x = 0.10$ , and d  $x = 0.15$

**Fig. 3** Plots of  $(\alpha h\nu)^2$  vs.  $h\nu$  of  $(\text{In}_{0.95-x}\text{Fe}_x\text{Sn}_{0.05})_2\text{O}_3$  thin films. The inset shows the optical bandgap of ITO thin film



attributed to the creation of oxygen-trapping centers. The number of oxygen-trapping centers increases on increasing the dopant concentration as they produce more charge carriers. This kind of decrease in optical bandgap on increasing the dopant concentration may be due to the creation of trapping centers as reported by Chen et al. [44]. They reported it as increased exchange interaction between valence band electrons of the host in sp shells and localized d electrons of the dopants.

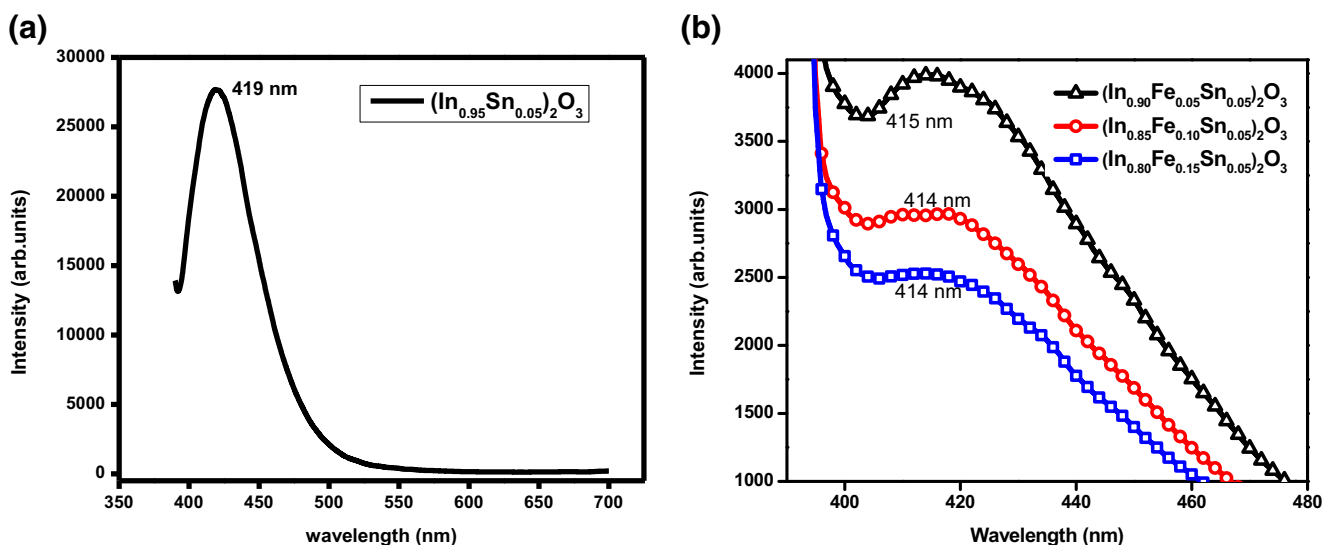
### 3.4 Photoluminescence Studies

Figure 4a, b shows the photoluminescence spectra of  $(\text{In}_{0.95-x}\text{Fe}_x\text{Sn}_{0.05})_2\text{O}_3$  thin films, at  $x = 0.00, 0.05, 0.1,$

and 0.15. The PL studies were carried out by a source having an excitation wavelength of 375 nm. A broad emission peak was observed in the ultraviolet region. The emission peak at 415 nm was observed for all Fe-doped ITO thin films. This is correlated to the combined emission peak related to glass and Fe:ITO. The intensity of PL peaks was found to decrease on increasing the Fe concentration due to their enhanced ability to capture photoelectrons [45].

### 3.5 XPS Studies

The XPS spectra for ITO and at  $x = 0.15$  Fe-doped ITO thin films were carried out to know the oxidation state of elements. The narrow XPS scan spectra for indium (In) are



**Fig. 4** a, b PL plots of a  $(\text{In}_{0.90}\text{Sn}_{0.05})_2\text{O}_3$  thin film. b  $(\text{In}_{0.95-x}\text{Fe}_x\text{Sn}_{0.05})_2\text{O}_3$  thin films, where  $x = 0.05, 0.1,$  and 0.15

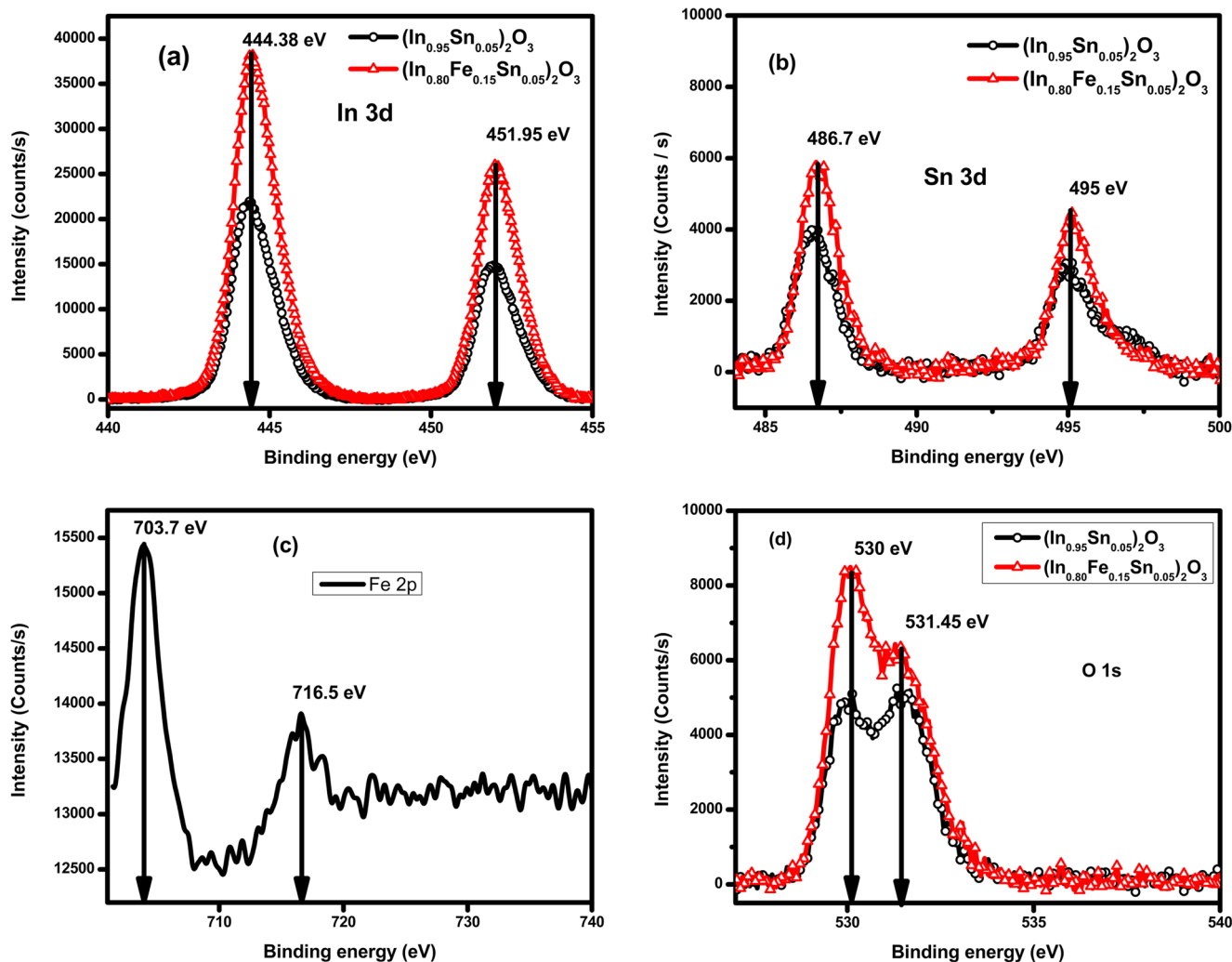


**Fig. 5** a–d XPS spectra of  $(\text{In}_{0.95-x}\text{Fe}_x\text{Sn}_{0.05})_2\text{O}_3$  thin films, where  $x = 0.00$  and  $0.15$ . **a** In3d spectra, **b** Sn3d spectra, **c** Fe2p spectra, and **d** O1s spectra

shown in Fig. 5a. Two peaks at 444.38 and 451.95 eV were observed. The peak at 444.38 eV is the binding energy of the  $3d_{5/2}$  state of the In3d shell. The peak at 451.95 eV is the binding energy of the  $3d_{3/2}$  state of the In3d shell. The observed binding energies of the In3d shell match the reported value [46]. This indicates the absence of In metal clusters and the presence of In in +3 state in both ITO and Fe:ITO thin films. The narrow XPS scan spectra for tin (Sn) are shown in Fig. 5b. It is found to be splitting into two binding energies of 487 and 495 eV. The peak at binding energy of 487 eV corresponds to the  $3d_{5/2}$  state of the Sn3d shell. The peak at the binding energy of 495 eV corresponds to the  $3d_{3/2}$  state of the Sn3d shell. The observed binding energy is in accordance with the literature [46]. The binding energy of Fe  $2p_{3/2}$  was found at 703.7 eV while that of Fe  $2p_{1/2}$  was observed at 717 eV as shown in Fig. 5c. There is a slight shift in binding energies of Fe 2p spectra when compared with the reported binding value [46]. This

suggests the Fe is present in two different states, i.e.,  $\text{Fe}^{2+}$  and  $\text{Fe}^{3+}$  in the sample. Even the oxygen spectra show two binding energy peaks corresponding to the oxygen present in  $\text{In}_2\text{O}_3$  at 530 eV, and the other one corresponds to the oxygen present in  $\text{SnO}_2$  at 531.45 eV. [47] in Fig. 5d.

### 3.6 Magnetic Studies

Figure 6a shows the field-dependent magnetization plot for  $(\text{In}_{0.95-x}\text{Fe}_x\text{Sn}_{0.05})_2\text{O}_3$  thin films, at  $x = 0.00, 0.05, 0.1$ , and  $0.15$  at 5 K under an applied field of  $\pm 20$  kOe. The diamagnetic background due to the substrate has been subtracted from the original data. The results show the existence of weak ferromagnetism at all concentrations of Fe.

The saturation magnetization ( $M_s$ ) decreased to 15 memu/cm<sup>3</sup> for Fe ( $x = 0.05$ ) doped in ITO. On further increase in doping concentration, the saturation

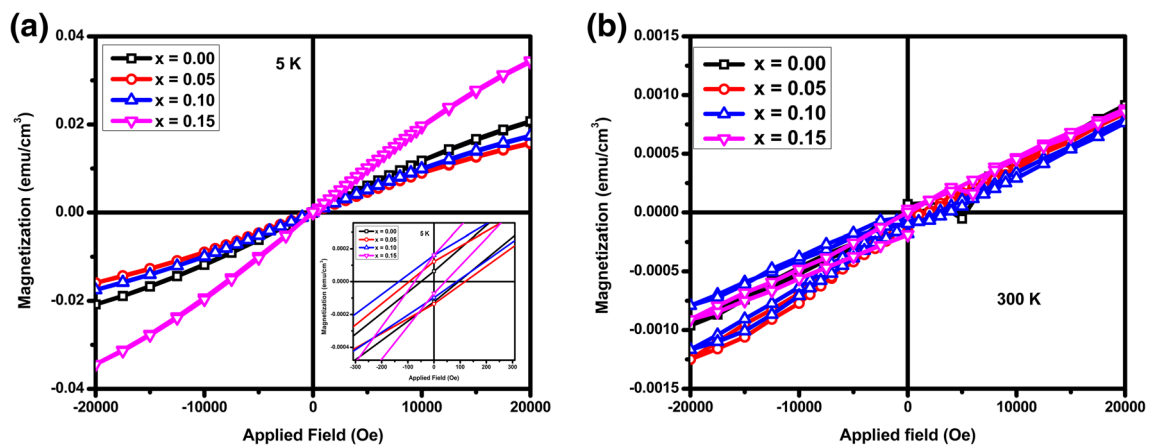


**Fig. 6** **a, b**  $M$ - $H$  plot of  $(\text{In}_{0.95-x}\text{Fe}_x\text{Sn}_{0.05})_2\text{O}_3$  thin films, where  $x = 0.00, 0.05, 0.1,$  and  $0.15$  at **a** 5 K (the inset shows the  $M$ - $H$  plot under  $\pm 200$  Oe) and **b** 300 K

magnetization was found to increase from 15 to 35  $\text{memu}/\text{cm}^3$ . The retentivity ( $M_r$ ) of the films increased from 0.06 to 0.163  $\text{memu}/\text{cm}^3$  on increasing the doping concentration from  $x = 0.00$  to  $x = 0.15$ . The coercivity ( $H_c$ ) decreased on increasing the dopant concentration. The summary of the magnetic parameter values at 5 K is reported in Table 1.

The films exhibited weak ferromagnetism at 5 K. This is due to the presence of hematite ion which exhibits canted antiferromagnetism in nanopowders [37]. So when those nanopowders exhibiting canted antiferromagnetism were coated and cooled to 5 K, the surface of the films may be mostly covered with canted spins with respect to the direction of field leading to weak ferromagnetism.

At room temperature, the weak ferromagnetism get reduced to paramagnetism for all concentrations of Fe-doped ITO thin films as shown in Fig. 6b under an applied field of  $\pm 20$  kOe. Hence, it has been observed that on an increase in temperature, the magnetic property of Fe-doped ITO thin films get degraded. Most of the researchers have reported ferromagnetism at room temperature in pure and doped ITO thin films [48–53]. All those reports correlate the existence of ferromagnetism to the presence of oxygen vacancies. The previous reports suggest that ferromagnetism in dilute magnetic semiconducting oxides

were because of oxygen vacancy as explained by the RKKY model.

In this case, the thicknesses of thin films were less than 400 nm but the oxygen vacancies were present. In spite of the presence of oxygen vacancy, the magnetic property for Fe-doped ITO thin films deteriorated. This indicates that the presence of oxygen vacancy is not the main criterion for exhibiting ferromagnetism at room temperature. As suggested for Cu-doped  $\text{CeO}_2$  thin films, the occurrence of ferromagnetism is also correlated to the arrangement of spins or elements in the surface of thin films by Bernardi et al. [54]. The presence of canted spin structure on the surface of thin films leads to the vanishing of long-range magnetic ordering. The clustering of these canted spins on the surface of thin films leads to chirality-induced paramagnetism [55]. They are said to obey Dzyaloshinskii-Moriya interaction (DM) [55–57]. Such kinds of materials were termed as skyrmions. The reason behind the paramagnetic nature in thin films while the

**Table 1** Summary of magnetic parameters for  $(\text{In}_{0.95-x}\text{Fe}_x\text{Sn}_{0.05})_2\text{O}_3$  thin films, where  $x = 0.00, 0.05, 0.1,$  and  $0.15$  at 5 K

Sample	$M_s$ ( $\text{emu}/\text{cm}^3$ )	$M_r$ ( $\text{memu}/\text{cm}^3$ )	$H_c$ (Oe)
$x = 0.00$	0.020	0.06	93
$x = 0.05$	0.015	0.120	121.03
$x = 0.10$	0.017	0.165	87.57
$x = 0.15$	0.035	0.165	43.15

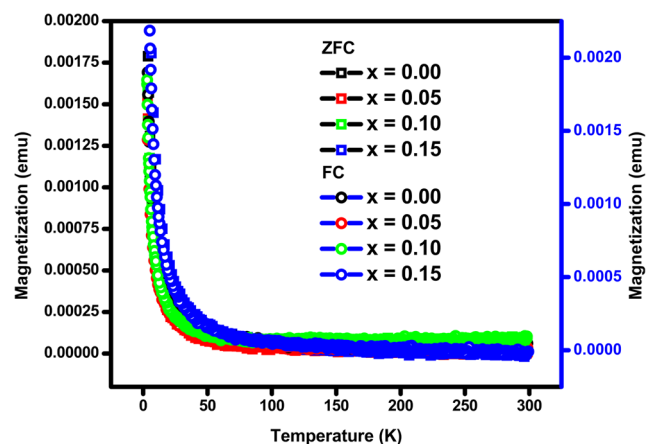
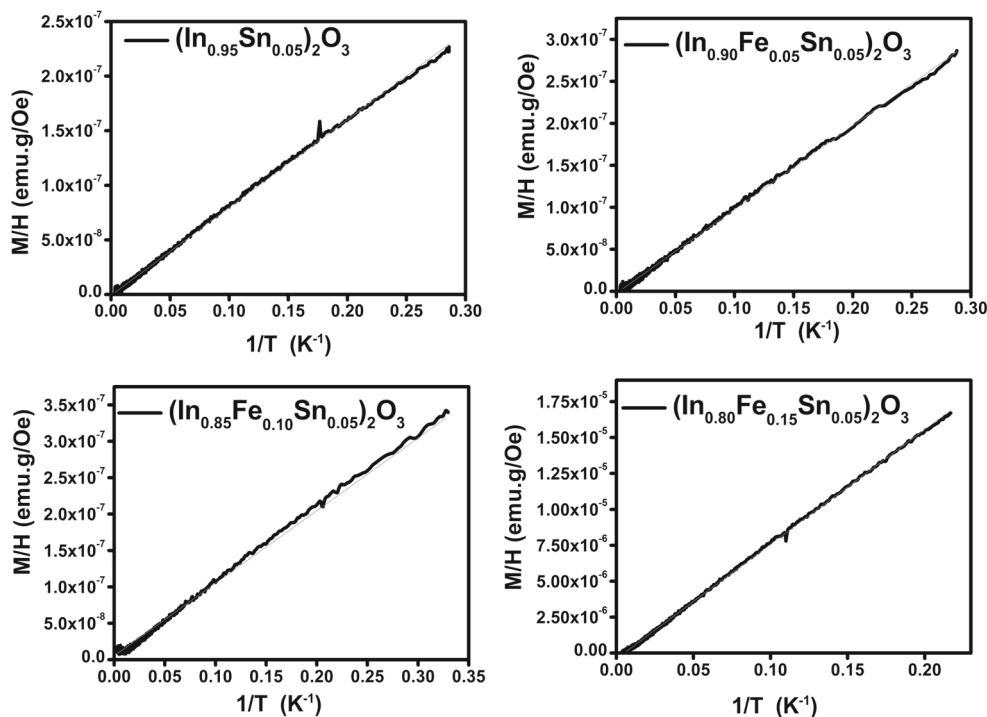


**Fig. 7** ZFC-FC plot of  $(\text{In}_{0.95-x}\text{Fe}_x\text{Sn}_{0.05})_2\text{O}_3$  thin films, where  $x = 0.00, 0.05, 0.1,$  and  $0.15$  at 1000 Oe

**Fig. 8** Curie law fitting plot of  $(\text{In}_{0.95-x}\text{Fe}_x\text{Sn}_{0.05})_2\text{O}_3$  thin films, where  $x = 0.00, 0.05, 0.1,$  and  $0.15$



nanopowders showed canted antiferromagnetism at room temperature is the deposition of canted spins on the surface of the thin films. As the Fe:ITO nanopowders exhibited canted antiferromagnetism at room temperature, it may be possible that while coating the same nanopowders, the particles with canted spins get arranged in the surface of the substrate leading to the formation of chirality. When more than two canted antiferromagnetic spins cluster together, they were termed as skyrmions. These skyrmions exhibit paramagnetism at room temperature as reported by other groups [55–59]. The materials having skyrmionic property find application in memory track devices. Also, the films exhibited weak ferromagnetism at 5 K and when the films are heated to room temperature from 5 K, they became paramagnetic. This is because the canted spins will get more thermal vibration due to heat. This increase in thermal energy on the surface spins may lead to more randomness which is one of the main causes of paramagnetism. The same paramagnetic behavior is obtained in temperature-dependent magnetic measurement as shown in Fig. 7. The magnetization was found to be decreasing on increasing the

temperature. This kind of steep decrease in magnetization is due to the paramagnetic nature of all the samples.

The temperature-dependent magnetization measurement taken in the presence of the field was fitted using Curie law for all Fe-doped ITO thin films as shown in Fig. 8. The films were found to obey the Langevin theory of paramagnetism, which is extended to Curie’s law. According to Curie law,  $\chi = C/T$ . So,  $1/T$  vs.  $\chi$  were plotted for all concentrations of Fe-doped ITO films. The slope of linear fitting of all the plots gives the Curie constant. The effective magnetic moment ( $\mu_{\text{eff}}$ ) of films was calculated using the formula [60] derived from Curie’s law and Langevin theory of paramagnetism.

$$\mu_{\text{eff}} = \sqrt{\frac{3K_B C M_W}{N}} \mu_B \tag{4}$$

where  $K_B$  is the Boltzmann constant and  $C$  is the Curie constant,  $M_W$  is the molecular weight of the sample,  $N$  is Avogadro’s number, and  $\mu_B$  is the Bohr magneton.

The effective magnetic moment was found to increase from  $0.04 \mu_B$  per Fe ion to  $0.4 \mu_B$  per Fe ion on increasing

**Table 2** Summary of crystallite size, FWHM, lattice parameter, dislocation density, strain, and optical bandgap in  $(\text{In}_{0.95-x}\text{Fe}_x\text{Sn}_{0.05})_2\text{O}_3$  at  $x = 0.00, 0.05, 0.10,$  and  $0.15$  thin films

$(\text{In}_{0.95-x}\text{Fe}_x\text{Sn}_{0.05})_2\text{O}_3$	$D$ (nm)	$a$ (Å)	FWHM	$\delta * 10^{14} \text{ m}^{-2}$	$\epsilon * 10^{-4}$	$E_g$ (eV)	$\mu_{\text{eff}}$ ( $\mu_B$ )
$x = 0.00$	18	9.94	0.334	65.8	25.8	3.94	0.042
$x = 0.05$	18	10	0.357	56.2	25.3	3.87	0.046
$x = 0.10$	16	10	0.370	49.7	23.4	3.84	0.046
$x = 0.15$	30	10.01	0.34	18.4	14.1	3.81	0.407

the concentration of Fe. This is in accordance with the trend of magnetization obtained at 300 K. The effective magnetic moment for all films along with corresponding crystallite size, FWHM, lattice constant, strain, dislocation density and optical bandgap are summarized in Table 2.

## 4 Conclusion

Fe-doped ITO thin films with varying Fe concentrations were coated on glass substrate using the electron beam evaporation technique. The XRD data confirms the single-phase formation of all thin films with enhancement in crystallite size on increasing the dopant concentration. The optical bandgap is found to decrease from 3.94 to 3.81 eV on increasing the dopant concentration. The photoluminescence spectra show an emission peak at 415 nm with decreasing intensity on increasing the dopant concentration due to photocapturing of electrons. The XPS spectra show the related binding energies of all the compositional elements. This suggests that Fe is present in two different oxidation states, at +2 and +3 states. The Fe:ITO thin films exhibit paramagnetism at room temperature due to the deposition of canted spin particles on the surface of thin films. The films obey the Langevin theory of paramagnetism. The effective magnetic moment ( $\mu_{\text{eff}}$ ) increased from 0.04 ( $\mu_B$ ) to 0.4 ( $\mu_B$ ) on increasing the concentration of Fe ion.

**Acknowledgments** The authors are grateful to UGC-DAE-CSR, IGCAR, Kalpakkam, 603102, Tamil Nadu, India, for providing financial support under Project Sanction number (CSR-KN/CRS-72/2015-2016/809) to carry out the present work. The authors are very thankful to VIT-SIF for providing XRD and DRS facilities to carry out the present work. The authors are grateful to National Physical Laboratory (NPL, New Delhi) for providing the PL spectrophotometer. The authors are also thankful to UGC-DAE-CSR, IGCAR, for providing VSM facility.

## References

- Freeman, A.J., Poepelmeier, K.R., Mason, T.O., Chang, R.P.H., Marks, T.J.: MRS Bull. <https://doi.org/10.1557/mrs2000.150> (2011)
- Granqvist, C.G.: Appl. Phys. A. <https://doi.org/10.1007/BF00323721> (1991)
- Granqvist, C.G., Hultåker, A.: Thin Solid Films. [https://doi.org/10.1016/S0040-6090\(02\)00163-3](https://doi.org/10.1016/S0040-6090(02)00163-3) (2002)
- Hamberg, I., Granqvist, C.G.: J. Appl. Phys. <https://doi.org/10.1063/1.337534> (1986)
- Kiliç, Ç., Zunger, A.: Phys. Rev. Lett. <https://doi.org/10.1103/PhysRevLett.88.095501> (2002)
- Lewis, B.G., Paine, D.C.: MRS Bull. <https://doi.org/10.1557/mrs2000.147> (2011)
- Phillips, J.M., Cava, R.J., Thomas, G.A., Carter, S.A., Kwo, J., Siegrist, T., Krajewski, J.J., Marshall, J.H., Peck, W.F., Rapkine, D.H.: Appl. Phys. Lett. <https://doi.org/10.1063/1.115118> (1995)
- Wang, R., King, L.L.H., Sleight, A.W.: J. Mater. Res. <https://doi.org/10.1557/JMR.1996.0208> (2011)
- Nomura, K., Ohta, H., Ueda, K., Kamiya, T., Hirano, M., Hosono, H.: Science. <https://doi.org/10.1126/science.1083212> (2003)
- Azevedo, S., Diéguez, L., Carvalho, P., Carneiro, J.O., Teixeira, V., Martínez, E., Samitier, J.: J Nano Res **17**, 75 (2012)
- Li, X., Li, C., Wang, D., Pradeep, C., Furuta, M., Hatta, A.: In: 2013 Twentieth International Workshop on Active-Matrix Flatpanel Displays and Devices (AM-FPD), pp 177–180 (2013)
- Alam, M.J., Cameron, D.C.: Thin Solid Films. [https://doi.org/10.1016/S0040-6090\(00\)01369-9](https://doi.org/10.1016/S0040-6090(00)01369-9) (2000)
- Chamberlin, R.R., Skarman, J.S.: J. Electrochem. Soc. **113**, 86 (1966)
- Danson, N., Safi, I., Hall, G.W., Howson, R.P.: Surf. Coat. Technol. [https://doi.org/10.1016/S0257-8972\(97\)00436-2](https://doi.org/10.1016/S0257-8972(97)00436-2) (1998)
- Furuta, M., Kawaharamura, T., Wang, D., Toda, T., Hirao, T.: IEEE Electron Dev. Lett. <https://doi.org/10.1109/LED.2012.2192902> (2012)
- Geoffroy, C., Campet, G., Portier, J., Salardenne, J., Couturier, G., Bourrel, M., Chabagno, J.M., Ferry, D., Quet, C.: Thin Solid Films. [https://doi.org/10.1016/0040-6090\(91\)90543-7](https://doi.org/10.1016/0040-6090(91)90543-7) (1991)
- Seo, H., Aihara, S., Watabe, T., Ohtake, H., Sakai, T., Kubota, M., Egami, N., Hiramatsu, T., Matsuda, T., Furuta, M., Hirao, T.: Jpn. J. Appl. Phys. **50**, 024103 (2011)
- Jin, Z.-C., Hamberg, I., Granqvist, C.G.: Appl. Phys. Lett. <https://doi.org/10.1063/1.99008> (1987)
- Kim, J.S., Granström, M., Friend, R.H., Johansson, N., Salaneck, W.R., Daik, R., Feast, W.J., Cacialli, F.: J. Appl. Phys. <https://doi.org/10.1063/1.368981> (1998)
- Kulaszewicz, S.: Thin Solid Films. [https://doi.org/10.1016/0040-6090\(81\)90070-5](https://doi.org/10.1016/0040-6090(81)90070-5) (1981)
- Lippens, P., Segers, A., Haemers, J., De Gryse, R.: Thin Solid Films. [https://doi.org/10.1016/S0040-6090\(97\)00632-9](https://doi.org/10.1016/S0040-6090(97)00632-9) (1998)
- Maki, K., Komiya, N., Suzuki, A.: Thin Solid Films. <https://doi.org/10.1016/j.tsf.2003.08.021> (2003)
- Furuta, M., Kamada, Y., Hiramatsu, T., Li, C., Kimura, M., Fujita, S., Hirao, T.: Jpn. J. Appl. Phys. **50**, 03CB09 (2011)
- Maruyama, T., Fukui, K.: Thin Solid Films. [https://doi.org/10.1016/0040-6090\(91\)90137-M](https://doi.org/10.1016/0040-6090(91)90137-M) (1991)
- Mattox, D.M.: Thin Solid Films. [https://doi.org/10.1016/0040-6090\(91\)90491-F](https://doi.org/10.1016/0040-6090(91)90491-F) (1991)
- Mayer, B.: Thin Solid Films. [https://doi.org/10.1016/0040-6090\(92\)90811-O](https://doi.org/10.1016/0040-6090(92)90811-O) (1992)
- Shanthi, E., Banerjee, A., Dutta, V., Chopra, K.L.: Thin Solid Films. [https://doi.org/10.1016/0040-6090\(80\)90160-1](https://doi.org/10.1016/0040-6090(80)90160-1) (1980)
- Sakai, T., Seo, H., Aihara, S., Kubota, M., Egami, N., Wang, D., Furuta, M.: Jpn. J. Appl. Phys. **51**, 010202 (2012)
- Vasu, V., Subrahmanyam, A.: Thin Solid Films. [https://doi.org/10.1016/0040-6090\(90\)90221-X](https://doi.org/10.1016/0040-6090(90)90221-X) (1990)
- Singhal, R.K., Samariya, A., Kumar, S., Sharma, S.C., Xing, Y.T., Deshpande, U.P., Shripathi, T., Saitovitch, E.: Appl. Surf. Sci. <https://doi.org/10.1016/j.apsusc.2010.07.106> (2010)
- Ma, R.-R., Jiang, F.-X., Qin, X.-F., Xu, X.-H.: Mater. Chem. Phys. <https://doi.org/10.1016/j.matchemphys.2011.12.014> (2012)
- Xiao, Z.R., Fan, X.F., Guan, L.X., Huan, C.H.A., Kuo, J.L., Wang, L.: J. Phys. Condens. Matter **21**, 272202 (2009)
- Wu, K., Gu, S., Tang, K., Zhu, S., Zhou, M., Huang, Y., Xu, M., Zhang, R., Zheng, Y.: Physica B: Condens. Matter. <https://doi.org/10.1016/j.physb.2012.03.040> (2012)
- Yu, Z.G., He, J., Xu, S., Xue, Q., van't Erve, O.M.J., Jonker, B.T., Marcus, M.A., Yoo, Y.K., Cheng, S., Xiang, X.-D.: Phys. Rev. B. <https://doi.org/10.1103/PhysRevB.74.165321> (2006)
- Harinath Babu, S., Kaleemulla, S., Madhusudhana Rao, N., Krishnamoorthi, C.: J. Magn. Magn. Mater. <https://doi.org/10.1016/j.jmmm.2016.05.007> (2016)



36. Huang, L.M., Moysés Araújo, C., Ahuja, R.: *Eur. Phys. Lett.* **87**, 27013 (2009)
37. Chakraborty, D., Kaleemulla, S., Madhusudhana Rao, N., Venugopal Rao, G.: *J. Mater. Sci. Mater. Electron.* <https://doi.org/10.1007/s10854-017-7851-0> (2017)
38. Cullity, B.D.: *Elements of X-Ray Diffraction*, p. 78. Addison-Wesley, Reading (1972)
39. Lagerstedt, O., Monemar, B.: *Phys. Rev. B.* <https://doi.org/10.1103/PhysRevB.19.3064> (1979)
40. Leszczyński, M., Litwin-Staszewska, E., Suski, T., Bąk-Misiuk, J., Domagała, J.: *Acta Phys. Pol. A* **88**, 837 (1995)
41. Sen, S., Halder, S.K., Sen Gupta, S.P.: *J. Phys. Soc. Jpn.* <https://doi.org/10.1143/JPSJ.38.1641> (1975)
42. Pathinettam Padiyan, D., Marikani, A., Murali, K.R.: *Mater. Chem. Phys.* [https://doi.org/10.1016/S0254-0584\(02\)00211-0](https://doi.org/10.1016/S0254-0584(02)00211-0) (2003)
43. Fallah, H.R., Ghasemi, M., Hassanzadeh, A., Steki, H.: *Mater. Res. Bull.* <https://doi.org/10.1016/j.materresbull.2006.06.024> (2007)
44. Chen, Z.C., Zhuge, L.J., Wu, X.M., Meng, Y.D.: *Thin Solid Films.* <https://doi.org/10.1016/j.tsf.2007.01.015> (2007)
45. Xin, B.F., Jing, L.Q., Fu, H.G., Sun, Z.H., Ren, Z.Y., Wang, B.Q., Cai, W.M.: *Gaodeng Xuexiao Huaxue Xuebao/Chem. J. Chin. Univ.* <https://doi.org/10.1016/j.jssc.2004.05.064> (2004)
46. Chastain, J., King, R.C., Moulder, J.: *Handbook of X-ray photoelectron spectroscopy: a reference book of standard spectra for identification and interpretation of XPS data* (Physical Electronics Division). Perkin-Elmer Corporation Eden Prairie, Minnesota (1992)
47. Majumdar, H.S., Majumdar, S., Tobjörk, D., Österbacka, R.: *Synth. Met.* <https://doi.org/10.1016/j.synthmet.2009.04.010> (2010)
48. An, Y., Xing, Y., Pan, F., Wu, Z., Liu, J.: *Phys. Chem. Chem. Phys.* <https://doi.org/10.1039/C6CP01315E> (2016)
49. Jiang, F.-X., Xi, S.-B., Ma, R.-R., Qin, X.-F., Fan, X.-C., Zhang, M.-G., Zhou, J.-Q., Xu, X.-H.: *Chin. Phys. Lett.* **30**, 047501 (2013)
50. Khan, G.G., Ghosh, S., Sarkar, A., Mandal, G., Mukherjee, G.D., Manju, U., Banu, N., Dev, B.N.: *J. Appl. Phys.* <https://doi.org/10.1063/1.4928952> (2015)
51. Stankiewicz, J., Villuendas, F., Bartolomé, J.: *Phys. Rev. B.* <https://doi.org/10.1103/PhysRevB.75.235308> (2007)
52. Xia, B., Wu, Y., Ho, H.W., Ke, C., Song, W.D., Huan, C.H.A., Kuo, J.L., Zhu, W.G., Wang, L.: *Phys. B Condens. Matter.* <https://doi.org/10.1016/j.physb.2011.05.016> (2011)
53. Yoo, Y.K., Xue, Q., Lee, H.-C., Cheng, S., Xiang, X.D., Dionne, G.F., Xu, S., He, J., Chu, Y.S., Preite, S.D., Lofland, S.E., Takeuchi, I.: *Appl. Phys. Lett.* <https://doi.org/10.1063/1.1854720> (2005)
54. Bernardi, M.I.B., Mesquita, A., Beron, F., Pirota, K.R., de Zevallos, A.O., Doriguetto, A.C., de Carvalho, H.B.: *Phys. Chem. Chem. Phys.* <https://doi.org/10.1039/C4CP04879B> (2015)
55. Pappas, C., Lelièvre-Berna, E., Falus, P., Bentley, P.M., Moskvina, E., Grigoriev, S., Fouquet, P., Farago, B.: *Phys. Rev. Lett.* <https://doi.org/10.1103/PhysRevLett.102.197202> (2009)
56. Leonov, A.A., Bogdanov, A.N., Röbber, U.K.: *arXiv preprint* (2010)
57. Wilson, M.N., Butenko, A.B., Bogdanov, A.N., Monchesky, T.L.: *Phys. Rev. B.* <https://doi.org/10.1103/PhysRevB.89.094411> (2014)
58. Tokunaga, Y., Yu, X.Z., White, J.S., Rønnow, H.M., Morikawa, D., Taguchi, Y., Tokura, Y.: *Nat. Commun.* <https://doi.org/10.1038/ncomms8638> (2015)
59. Wiesendanger, R.: *Nat. Rev. Mater.* <https://doi.org/10.1038/natrevmats.2016.44> (2016)
60. Akyol, M., Ekicibil, A., Kıymaç, K.: *J. Supercond. Nov. Magn.* <https://doi.org/10.1007/s10948-013-2135-2> (2013)